

Nonlinear Two-Photon Absorption in the Near-Infrared Band for Lead Bromide Perovskite Films Using an F-Scan Nonlinear Spectrometer

Edgar Rueda,* Juan Serna, Jose Ignacio Uribe, Daniel Ramírez, Franklin Jaramillo, Jaime Osorio, and Hernando García*



Cite This: *ACS Omega* 2022, 7, 29100–29105



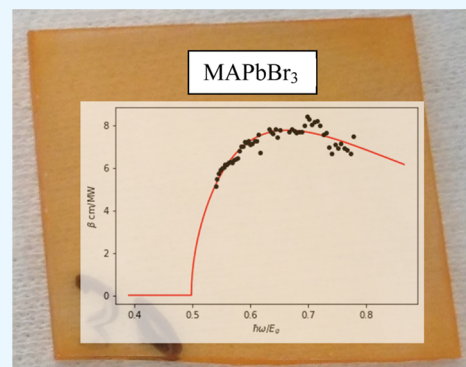
Read Online

ACCESS |

Metrics & More

Article Recommendations

ABSTRACT: An F-scan nonlinear spectrometer is used to measure the two-photon absorption coefficient for $\text{CH}_3\text{NH}_3\text{PbBr}_3$ perovskite films from 690 to 995 nm. This spectrometer uses an electrically focused tunable lens and a tunable femtosecond-pulse laser (Mai Tai-HP) with a resolution of 5 nm. Two-band models and saturation irradiance corrections are used to fit the experimental data. The nonlinear absorption in this wavelength range is of the order of cm/MW . We found that the best agreement between the experimental data, the reported values in the literature, and the theoretical model is obtained for an extended two-band model with irradiance saturation correction.



1. INTRODUCTION

Lead halide perovskites have emerged as desirable materials due to their particular optical and transport properties,^{1,2} leading to the fabrication of high-performance solar cells and, more recently, light-emitting diodes (LEDs)^{3,4} and batteries.⁵ The typical structure of a three-dimensional (3D) perovskite is ABX_3 , being A an organic molecule such as methylammonium CH_3NH_3 (MA), or formamidinium (FA), or an inorganic cation such as cesium (Cs). Lead (Pb) is commonly used in the B position, while I, Br, and Cl are used as X site anions. Combinations of these different atoms have been used to tune the bandgap and material stability.⁶ Metal halide perovskites have received attention due to significant advances in the increment of efficiency in photovoltaic devices,⁷ the defect-tolerant characteristic produced onto the material structure, and remarkable optoelectronic properties such as high absorption coefficient and high photoluminescence in the linear regime.

On the other hand, nonlinear optical properties have been less studied, but reports show large third-order optical nonlinearities on thin-film halide perovskites; thus, there is enormous viability for applications in photonic devices.^{8–12} In particular, Zhou et al.⁸ listed the measured values of two-photon absorption (TPA) for MAPbBr_3 perovskites found in the literature, with values in the order of cm/GW for single crystals and in the order of cm/MW for films. The nonlinear optical measurements in these reports were made for a specific

laser wavelength, yet it is desirable to measure these properties over a broader range of wavelengths to analyze some of the mechanisms that contribute to the nonlinear properties. In this work, we have been able to measure the nonlinear two-photon absorption (TPA) β of $\text{CH}_3\text{NH}_3\text{PbBr}_3$ thin-film perovskite in the near-infrared band, from 690 to 995 nm with a step of 5 nm using a recently proposed nonlinear absorption spectrometer (NAS) reported in ref 13, which is based on the TF-scan technique.^{14,15} The first part of Section 2 explains the technique used to fabricate the samples and present the physical and linear optical properties. In the second part of Section 2, we explain the working principle of the nonlinear spectrometer. In Section 3, first, we present the experimental results for the nonlinear two-photon absorption, and, second, we fit the data using two-band models. Finally, we analyze the results and give conclusions.

2. MATERIALS AND METHODS

2.1. Fabrication and Characterization Methods of Perovskite Films.

For this work, films were prepared

Received: May 12, 2022

Accepted: July 25, 2022

Published: August 9, 2022



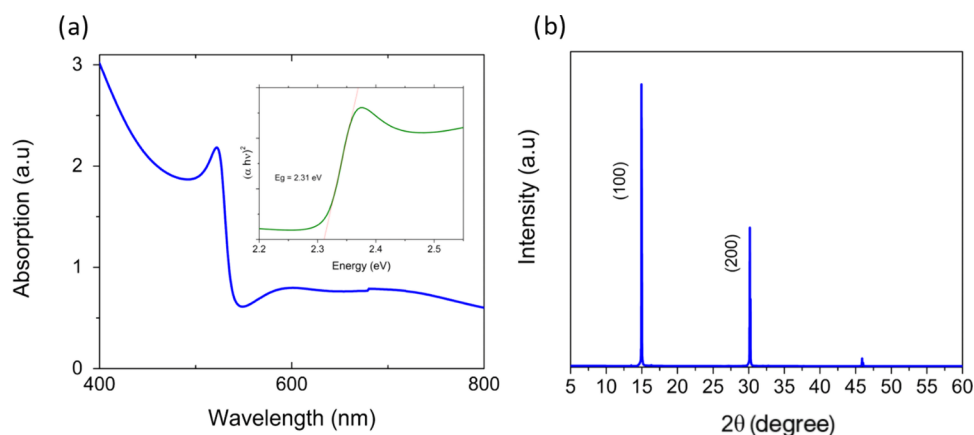


Figure 1. (a) Absorbance of MAPbBr₃; the inset shows the Tauc plot with the calculated energy gap. (b) XRD pattern of the MAPbBr₃ films.

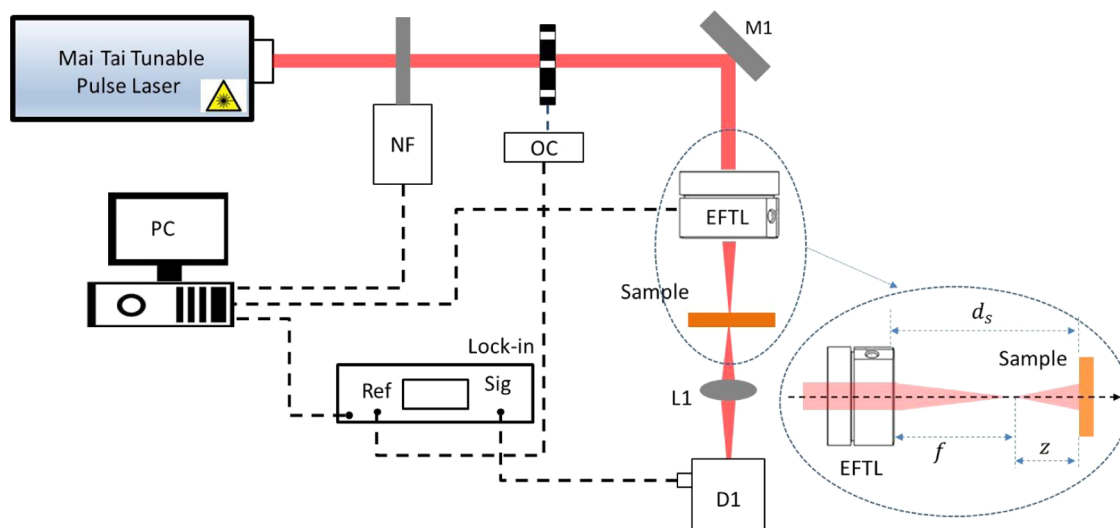


Figure 2. Experimental setup for the nonlinear spectrometer. (Laser source) Mai Tai spectra-physics tunable pulsed laser, NF is the neutral density filter, OC is the optical chopper, EFTL is the electrically focused tunable lens, and M1 is a mirror. The inset shows the experimental parameters used in the theoretical calculation for TPA.

according to the method reported in ref 5. Methylammonium bromide (MABr) from dyesol was used as an organic cation. Dimethyl sulfoxide (DMSO, Sigma-Aldrich) and *N,N*-dimethylformamide (DMF, Alfa Aesar) were used as solvents, with lead bromide (PbBr₂) (Alfa Aesar) as the lead source. To obtain MAPbBr₃, the precursor solution was deposited on top of 2.5 cm × 2.5 cm glass substrates by spin coating at 4000 rpm for 25 s. After 10 s of spin coating, 500 μL of diethyl ether was dropped to remove the DMF quickly. The films were then annealed at 65 °C for 1 min plus 100 °C for 10 min. Absorption measurements were taken in a Cary 100 Varian X-ray diffractogram in a PANalytical diffractometer. Samples were scanned from 2θ = 5 to 60° in a Bragg-Brentano geometry, using Cu Kα (1.5408 Å) radiation with a step size of 0.04° and a speed of 5 degree/min. Figure 1a shows the absorption spectrum of the MAPbBr₃ film; the particular excitonic characteristic of the Br perovskite is observed near 521 nm. The absorption values near high wavelengths can be attributed to scattering due to the film's roughness. The Tauc plot from the absorption data is presented in the inset. By extrapolating the linear region of the absorption coefficient, the electronic bandgap energy is estimated to be 2.31 ± 0.01 eV. Figure 1b shows the characteristic signal of MAPbBr₃

perovskite in its cubic phase. A scanning electron microscopy (SEM) image of a MAPbBr₃ film fabricated with the same technique can be observed in Figure 1c in ref 5, showing a smooth morphology with faint grain boundaries.

2.2. Nonlinear Optical Spectrometry in the Near-Infrared Region. A simplified scheme of an F-scan nonlinear spectrometer¹³ is depicted in Figure 2. The laser pulse is modulated with an optical chopper and filtered with a computer-controlled neutral filter (NF). The light then impinges onto an electrically focused tunable lens (EFTL) that focalizes and defocalizes the beam on the thin-film sample of study. The sample is placed at a fixed position d_s inside the range of the EFTL. All light transmitted through the sample, including scattered light, is collected and detected with a lens (L1) and an integrating sphere (D1). This light is then used to determine the two-photon absorption (TPA) coefficient.

For the experimental implementation, we used a Mai Tai tunable laser with a repetition rate of 80 MHz, an average pulse width of 75 fs, and laser emission from 690 to 995 nm, with a resolution of 5 nm. Respecting the use of high repetition lasers in measurements of TPA, several studies have addressed concerns about the correctness of the measurement,^{16,17} particularly regarding the existence of cumulative thermal

effects due to linear absorption.^{16,18–21} To address this problem, blanking has been suggested.^{18,19,22,23} Blanking allows the material to transfer the heat before a new train of pulses arrives by blocking the laser beam periodically. Thus, because we are already using a 50% duty cycle optical chopper to modulate light for the lock-in amplifier, as stated by Nag et al.,²³ to avoid thermal effects the chopper frequency has to be greater than $4D/2w_0^2$, where D is the thermal diffusion coefficient and w_0 is the beam waist at the sample. In our experiment, $w_0 \approx 0.016$ mm, $D = 0.145$ mm²/s,²⁴ and the frequency used is approximately 1130 Hz. Possible effects regarding light polarization^{19,25} were not addressed in this work. At the entrance surface of the sample, the average power was 20 mW and the irradiance varied as shown in Figure 3.

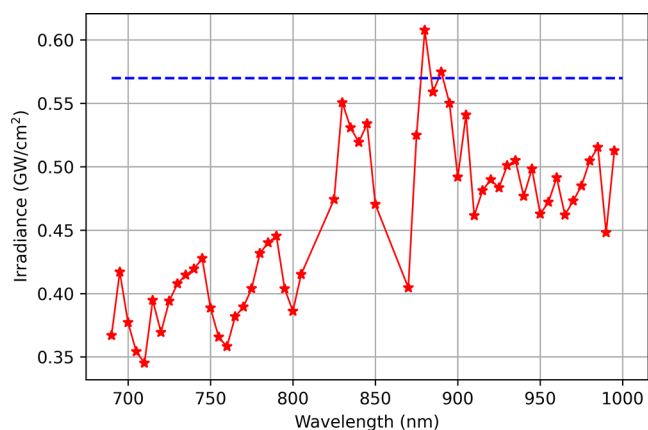


Figure 3. Irradiance I_0 at the entrance surface of the sample as a function of wavelength. The blue dashed line corresponds to the saturation irradiance I_{sat} for MAPbBr₃.

The EFTL is an OPTOTUNE-1030, controlled by an OPTOTUNE lens driver that gives a maximum current of 300 mA with a resolution of 0.1 mA. We used an integrating sphere to measure the transmitted laser light. The light collected by the integrating sphere is sent to a STANFORD RESEARCH 830 dual-channel lock-in amplifier, controlled through a general purpose interface bus (GPIB).

The nonlinear absorption spectrometer uses an electronically focused tunable lens (EFTL), with tunable focal distance f , as a dynamic system to generate, for each wavelength, the corresponding transmittance signal of an F-scan setup at two particular points: the point of maximum absorption ($z = d_s - f = 0$), which corresponds to high-intensity (HI) irradiation, and the point of low-intensity (LI) irradiation ($z = d_s - f \rightarrow \infty$), the region where nonlinear effects are negligible. Using the conventional Z-scan open-aperture expression for the transmittance,²⁶ we can obtain an expression for the transmittance of light through the sample as a function of $z = d_s - f$:

$$T(z) = 1 - \frac{\beta(1-R)I_0L_{\text{eff}}}{2\sqrt{2}(1+x^2)} \quad (1)$$

where I_0 is the irradiance in front of the sample, $R = (1-n)^2/(1+n)^2$ is the reflection coefficient at normal incidence, $n = 2.5$ is the typical refractive index of the perovskite samples, $L_{\text{eff}} = (1 - \exp(-\alpha L))/\alpha$ is the effective length, $\alpha = 450$ cm⁻¹²⁷ is the linear absorption coefficient (its effect is not significant and will be taken as constant in the whole wavelength range), $L = 1$

μm is the sample thickness, and $x = \frac{d_s - f}{z_0} = \frac{z}{z_0}$, with z_0 being the Rayleigh range.

When the conditions for HI and LI are applied in the transmittance equation (eq 1), we can find an expression for TPA as a function of wavelength λ

$$\beta(\lambda) = 2\sqrt{2} \left(1 - \frac{\text{LI}(\lambda)}{\text{HI}(\lambda)}\right) / (1-R)I_0(\lambda)L_{\text{eff}} \quad (2)$$

Saturation of the TPA coefficient has been observed due to irradiance saturation.^{27–29} To take into account this effect, we use eq 3 and the saturation value $I_{\text{sat}} = 0.57$ GW/cm² reported by Liu et al.²⁷

$$\beta(\lambda) = \frac{\beta_0(\lambda)}{1 + \left(\frac{I_0}{I_{\text{sat}}}\right)^2} \quad (3)$$

where β_0 is the nonsaturated TPA coefficient.

3. RESULTS AND DISCUSSION

3.1. Experimental Nonlinear Two-Photon Absorption.

The experimental TPA coefficients obtained with eq 2 correspond to the red dots in Figure 4. If we consider the

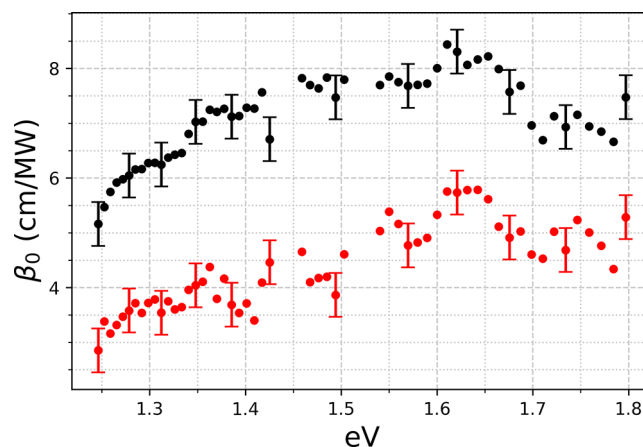


Figure 4. Two-photon absorption for a thin film of MAPbBr₃ perovskite, with a thickness of 1 μm . Black dots correspond to TPA with the saturation irradiance correction of eq 3. Red dots correspond to TPA without saturation irradiance correction.

correction proposed by Liu et al.²⁷ for a saturation irradiance of 0.57 GW/cm², using eq 3, the corrected TPA coefficient corresponds to the black dots in Figure 4. As shown in Figure 4, the correction scales the value of TPA by an approximately constant factor. Using the common uncertainty³⁰ measured for CdS in a previous study,¹³ for both curves, the estimated uncertainty is ± 0.4 cm/MW; the maximum value of TPA is around two-thirds of the energy gap, as expected.

3.2. Nonlinear Two-Photon Absorption Model. For MAPbI₃, Wei et al.³¹ report experimental TPA measurements without the characteristic maximum commonly observed in zinc blended semiconductors crystals at 0.7 times the bandgap energy of the material. Thus, they included relativistic effects induced by spin–orbit coupling to model this lack of a maximum. Nevertheless, by inspection of Figure 4, it is clear that for our MAPbBr₃ films, a maximum value of TPA exists around 0.7 times the bandgap energy. For this reason, we used two models based on the two-band model (TBM) presented in

Figure 5. In this model, we take into account a valence band with three bands corresponding to a light-hole (LH), a heavy-hole (HH), and a split-off band (SO).

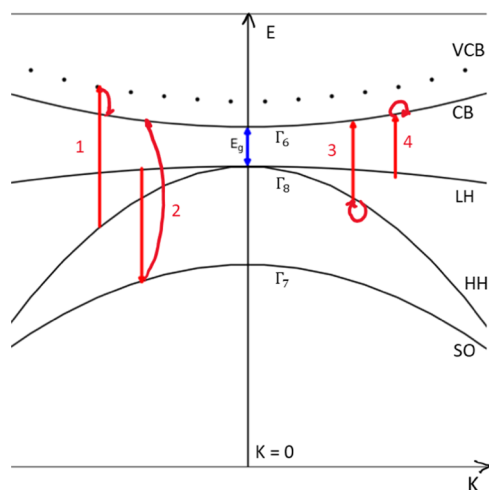


Figure 5. Assumed band structure as a zinc-blende to calculate the contribution to the TPA. The model includes a double-degenerate valence band with a light-hole (LH), heavy-hole (HH), and a split-off band (SO). In addition, in the conduction band, we proposed a virtual conduction band (VCB) to allow a forbidden–forbidden (f–f) transition. In the figure, possible transitions that may take place during the nonlinear absorption are shown.

heavy-hole band (HH), and a split-off band (SO). We also include transitions onto the conduction band (CB) and a possible virtual conduction band (VCB). The first model, called the two-band exciton model (TBEM), only considers allowed–forbidden (a–f) or forbidden–allowed (f–a) transitions, and includes a scaling law proposed by Van Stryland et al.,^{32,33} and an exciton effect correction for single crystals proposed by Ohara et al.³⁴ Equation 4 corresponds to the TBEM,

$$\beta = CA \frac{\sqrt{E_p} (2\hbar\omega/E_g - 1)^{3/2}}{n^2 E_g^3 (2\hbar\omega/E_g)^5} \quad (4)$$

where A is the scaling factor for β , E_g is the bandgap energy in eV, $\hbar\omega$ is the photon energy in eV, E_p is the Kane momentum energy (approximately 20 eV for direct bandgap materials), and C is the Sommerfeld factor

$$C(\hbar\omega) = \frac{x e^x}{\sin hx} \quad (5)$$

where $x = \pi \sqrt{E_b / (2\hbar\omega - E_g)}$ and E_b is the exciton binding energy in eV.

The second model proposed by Garcia et al.,³⁵ named the generalized TBM (GTBM), includes allowed–allowed (a–a), a–f, f–a, and forbidden–forbidden (f–f) transitions; some examples of these transitions are sketched in Figure 5: 1 for f–f, 2 for a–a, 3 for f–a, and 4 for a–f. Equation 6 corresponds to the GTBM

$$\beta = A \frac{\sqrt{E_p}}{n^2 E_g^3} \sum_{n=1}^3 f_n \frac{(2\hbar\omega/E_g - 1)^{1/2+n}}{(2\hbar\omega/E_g)^5} \quad (6)$$

where $n = 0, 1, \text{ or } 2$ correspond to a–a, a–f (or f–a), and f–f transitions, respectively. $f_n \leq 1$ is a numerical factor that

depends on the angular averages of the interband matrix elements that are going to be used here as fitting parameters.

Using the nonlinear least square method (python `scipy.optimize.curve_fit`), we have fitted the experimental data restricting the value of the bandgap energy to one-standard deviation (2.30–2.32 eV) and allowing the scaling factor to be as much as 40% below the accepted range (between 1940 and 5200).³⁶ If we consider the irradiance saturation of 0.57 GW/cm² and use an exciton binding energy of 20 meV,³⁷ the TBEM model will predict the blue dash-dotted curve of Figure 6 for parameters $A = 1880$ cm/MW and

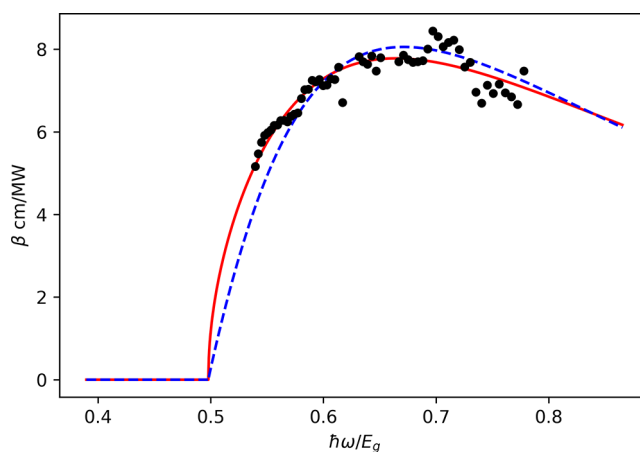


Figure 6. Fitting of the experimental (black dots) TPA coefficients corrected with eq 3 (black dots in Figure 4). Fit with a TBEM model (blue dashed line) and a GTBM model (red line).

$E_g = 2.30$ eV. The scaling factor A has the expected numerical value but in cm/MW. To evaluate the quality of the fit, we calculated the reduced chi-squared statistic, finding a $\chi^2_\nu = 1.6$, with a probability of finding a better fit of more than 99%, corresponding to a very poor fitting. In contrast, the GTBM model predicts the red curve with reduced chi-square statistic of $\chi^2_\nu = 0.6$, corresponding to a probability of finding a better fit of only 2%; thus, it is an excellent fit. The fitting parameters are $A = 2360$ cm/MW, $E_g = 2.30$ eV, $f_1 = 0.13$, $f_2 = 0.77$, and $f_3 = 0.24$, meaning that the main contribution is from the a–f and f–a transitions, while the a–a and f–f transitions contribute less. Again, the scaling factor A has the expected numerical value but in cm/MW.

Now, when ignoring any possible irradiance saturation, the fitting result can be seen in Figure 7. Using an exciton binding energy of 20 meV,³⁷ the TBEM model will predict the blue dash-dotted curve for parameters $A = 1182$ cm/MW and $E_g = 2.31$ eV. The scaling factor A is below the expected numerical value. The reduced chi-squared statistic is $\chi^2_\nu = 1.7$, with a probability of finding a better fit of more than 99%, which corresponds to a very poor fit. The GTBM model predicts the red curve with a reduced chi-square statistic of $\chi^2_\nu = 1.0$, corresponding to a probability of finding a better fit of only 62%; thus, it is a poor fit. For this case, the fitting parameters are $A = 2100$ cm/MW, $E_g = 2.30$ eV, $f_1 = 0.10$, $f_2 = 0.22$, and $f_3 = 0.93$, meaning that the main contribution is from the f–f transition.

On behalf of the scattering of the data around the fitting curves, the smaller chi-square statistic, and the fact that an a–f (f–a) transition is more plausible than an f–f transition, we believe that the correct experimental values correspond to

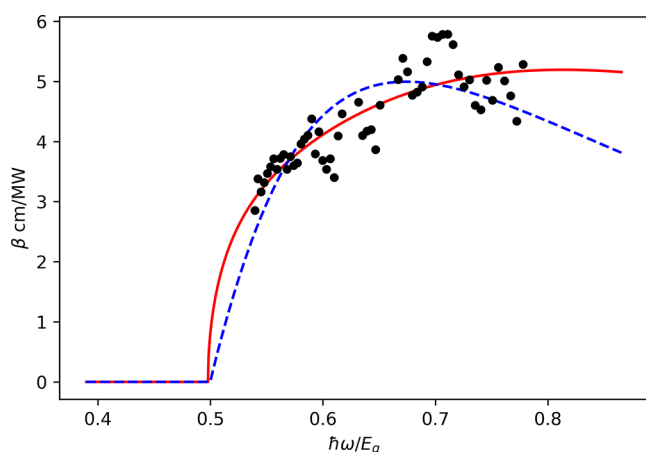


Figure 7. Fitting of the experimental (black dots) TPA coefficients without saturation correction (red dots in Figure 4). Fit with a TBEM model (blue dash-dotted line) and a GTBM model (red line).

those with irradiance saturation correction (Figure 6), and the correct model corresponds to the GTBM. Liu et al.²⁷ reported a TPA of $\beta_0 = 5.5$ cm/MW for a MAPbBr₃ film with a thickness of 0.38 μm at 800 nm. Although bigger, our value is of the same order, $\beta_0 = 7.8 \pm 0.4$ cm/MW. Because Liu et al. do not report any uncertainty, we follow the rule of Hughes and Hase³⁰ and take 0.1 cm/MW for the uncertainty in the value reported by Liu et al., which becomes 5.5 ± 0.1 cm/MW. We find that measuring the statistical distance between the values is 5.6 deviations; thus, they cannot be considered equal without a statistical doubt. Despite the disagreement with the value reported by Liu et al., it is important to remember that they did not report an uncertainty; if we suppose a 15% relative error, like in our data, the statistical distance reduces to only 2.5 deviations.

4. CONCLUSIONS

In conclusion, we have obtained an experimental dispersion curve for the two-photon absorption coefficient of MAPbBr₃ three-dimensional hybrid perovskite in a wavelength range of 690–995 nm, using a nonlinear absorption spectrometer based on an F-scan technique. We have found that the experimental TPA values corrected for irradiance saturation give the best possible fit, agreeing with the accepted fitting, and experimental parameters. We have found that the generalized two-band model of Garcia et al.³⁵ agrees with the measured bandgap and TPA values. Finally, the result shows that the most dominant contributions are from the a–f and f–a transitions but that the f–f and a–a transitions are not negligible.

AUTHOR INFORMATION

Corresponding Authors

Edgar Rueda – Grupo de Óptica y Fotónica, Instituto de Física, Universidad de Antioquia UdeA, Medellín 050010, Colombia; orcid.org/0000-0002-0273-6914; Email: edgar.rueda@udea.edu.co

Hernando García – Department of Physics, Southern Illinois University Edwardsville, Edwardsville, Illinois 62026, United States; Email: hgarcia@siue.edu

Authors

Juan Serna – Grupo de Óptica y Espectroscopía, Centro de Ciencia Básica, Universidad Pontificia Bolivariana, Medellín 050031, Colombia

Jose Ignacio Uribe – Centro de Investigación, Innovación y Desarrollo de Materiales—CIDEMAT, Facultad de Ingeniería and Grupo de Estado Sólido, Instituto de Física, Universidad de Antioquia UdeA, Medellín 050010, Colombia; Ingeniush, Institución Universitaria Salazar y Herrera, Medellín 050034, Colombia

Daniel Ramírez – Centro de Investigación, Innovación y Desarrollo de Materiales—CIDEMAT, Facultad de Ingeniería, Universidad de Antioquia UdeA, Medellín 050010, Colombia; orcid.org/0000-0003-2630-7628

Franklin Jaramillo – Centro de Investigación, Innovación y Desarrollo de Materiales—CIDEMAT, Facultad de Ingeniería, Universidad de Antioquia UdeA, Medellín 050010, Colombia; orcid.org/0000-0003-1722-5487

Jaime Osorio – Grupo de Estado Sólido, Instituto de Física, Universidad de Antioquia UdeA, Medellín 050010, Colombia

Complete contact information is available at:

<https://pubs.acs.org/10.1021/acsomega.2c02967>

Notes

The authors declare no competing financial interest.

ACKNOWLEDGMENTS

D.R., F.J., and J.I.U. gratefully acknowledge the financial support provided by the Colombia Scientific Program within the framework of the call (Contract No. FP44842-218-2018). The authors thank the program “Estrategia de Sostenibilidad 2017–2019 de la Universidad de Antioquia”. J.S. acknowledges the support from Universidad Pontificia Bolivariana. E.R. thanks Universidad de Antioquia UdeA Estrategia de Sostenibilidad “ÓPTICA Y FOTÓNICA-Sostenibilidad 2020–2021”. J.S., E.R., and J.I.U. acknowledge the financial support provided by G8-(Acta 2020 3906) Universidad de Antioquia, Instituto Tecnológico Metropolitano, Universidad Pontificia Bolivariana, Institución Universitaria Salazar y Herrera and Ruta N. H. Garcia thanks Southern Illinois University, Edwardsville, for financial support.

REFERENCES

- (1) Stranks, S. D.; Eperon, G. E.; Grancini, G.; Menelaou, C.; Alcocer, M. J. P.; Leijtens, T.; Herz, L. M.; Petrozza, A.; Snaith, H. J. Electron-Hole Diffusion Lengths Exceeding 1 micrometer in an organometal trihalide perovskite absorber. *Science* **2013**, *342*, 341–344.
- (2) Leijtens, T.; Stranks, S. D.; Eperon, G. E.; Lindblad, R.; Johansson, E. M. J.; Ball, J. M.; Lee, M. M.; Snaith, H. J.; Mcpherson, I. J. Electronic Properties of Meso-Superstructured and Planar Organometal Halide Perovskite Films: Charge Trapping, Photodoing, and Carrier Mobility. *ACS Nano* **2014**, *7*, 7147–7155.
- (3) Zhao, X.; Zhang, B.; Zhao, R.; Yao, B.; Liu, X.; Liu, J.; Xie, Z. Simple and Efficient Green-Light-Emitting Diodes Based on Thin Organolead Bromide Perovskite Films via Tuning Precursor Ratios and Postannealing Temperature. *J. Phys. Chem. Lett.* **2016**, *7*, 4259–4266.
- (4) Yu, J. C.; Kim, D. B.; Jung, E. D.; Lee, B. R.; Song, M. H. High-Performance Perovskite Light-Emitting Diodes via Morphological Control of Perovskite Films. *Nanoscale* **2016**, *8*, 7036–7042.
- (5) Ramirez, D.; Suto, Y.; Rosero-Navarro, N. C.; Miura, A.; Tadanaga, K.; Jaramillo, F. Structural and Electrochemical Evaluation of Three- and Two-Dimensional Organohalide Perovskites and Their

- Influence on the Reversibility of Lithium Intercalation. *Inorg. Chem.* **2018**, *57*, 4181–4188.
- (6) Fu, Q.; Tang, X.; Huang, B.; Hu, T.; Tan, L.; Chen, L.; Chen, Y. Recent Progress on the Long-Term Stability of Perovskite Solar Cells. *Adv. Sci.* **2018**, *5*, No. 1700387.
- (7) Green, M. A.; Ho-Baillie, A.; Snaith, H. J. The Emergence of Perovskite Solar Cells. *Nat. Photonics* **2014**, *8*, 506–514.
- (8) Zhou, Y.; Huang, Y.; Xu, X.; Fan, Z.; Khurgin, J. B.; Xiong, Q. Nonlinear Optical Properties of Halide Perovskites and Their Applications. *Appl. Phys. Rev.* **2020**, *7*, No. 041313.
- (9) Autere, A.; Jussila, H.; Dai, Y.; Wang, Y.; Lipsanen, H.; Sun, Z. Nonlinear Optics with 2D Layered Materials. *Adv. Mater.* **2018**, *30*, No. 1705963.
- (10) Mirershadi, S.; Ahmadi-Kandjani, S.; Zawadzka, A.; Rouhbakhsh, H.; Sahraoui, B. Third Order Nonlinear Optical Properties of Organometal Halide Perovskite by Means of the Z-Scan Technique. *Chem. Phys. Lett.* **2016**, *647*, 7–13.
- (11) Wang, J.; Mi, Y.; Gao, X.; Li, J.; Li, J.; Lan, S.; Fang, C.; Shen, H.; Wen, X.; Chen, R.; Liu, X.; He, T.; Li, D. Giant Nonlinear Optical Response in 2D Perovskite Heterostructures. *Adv. Opt. Mater.* **2019**, *7*, No. 1900398.
- (12) Kalanoor, B. S.; Gouda, L.; Gottesman, R.; Tirosh, S.; Haltzi, E.; Zaban, A.; Tischler, Y. R. Third-Order Optical Nonlinearities in Organometallic Methylammonium Lead Iodide Perovskite Thin Films. *ACS Photonics* **2016**, *3*, 361–370.
- (13) Garcia, H.; Serna, J.; Rueda, E. Bulk ZnSe and CdS Two-Photon Absorption measurement with a F-Scan Non-Linear Absorption Spectrometer. *OSA Continuum* **2020**, *3*, 498–504.
- (14) Kolkowski, R.; Samoc, M. Modified Z-Scan Technique Using Focus-Tunable Lens. *J. Opt.* **2014**, *16*, No. 125202.
- (15) Rueda, E.; Serna, J. H.; Hamad, A.; Garcia, H. Two-Photon Absorption Coefficient Determination Using the Differential F-Scan Technique. *Opt. Laser Technol.* **2019**, *119*, No. 105584.
- (16) Makhal, K.; Mathur, P.; Maurya, S.; Goswami, D. Extracting Third Order Optical Nonlinearities of Mn (III) -Phthalocyanine Chloride Using High Repetition Rate Femtosecond Pulses. *J. Appl. Phys.* **2017**, *121*, No. 053103.
- (17) Edziah, R.; Lalanne, E.; Torres, V.; Johnson, A. M.; Trivedi, S. Z-Scan Measurements Using Ultrashort High-Repetition-Rate Lasers: How to Recognize the Parasitic Effects of Nonlinear Behavior of Fused-Silica Damage Sites. *J. Opt. Soc. Am. B* **2011**, *28*, 1385–1390.
- (18) De, A. K.; Goswami, D. Exploring the Nature of Photo-Damage in Two-Photon Excitation by Fluorescence Intensity Modulation. *J. Fluoresc.* **2009**, *19*, 381–386.
- (19) Goswami, D.; Nag, A. Exploring Control Parameters of Two Photon Processes in Solutions. *J. Chem. Sci.* **2012**, *124*, 281–289.
- (20) Kamada, K.; Matsunaga, K.; Yoshino, A.; Ohta, K. Two-Photon-Absorption-Induced Accumulated Thermal Effect on Femtosecond Z-Scan Experiments Studied with Time-Resolved Thermal-Lens Spectrometry and Its Simulation. *J. Opt. Soc. Am. B* **2003**, *20*, 529–537.
- (21) Gnoli, A.; Razzari, L.; Righini, M. Z-Scan Measurements Using High Repetition Rate Lasers: How to Manage Thermal Effects. *Opt. Express* **2005**, *13*, 7976–7981.
- (22) Maurya, S. K.; Dutta, C.; Goswami, D. Concentration Dependent Approach for Accurate Determination of Two-Photon Absorption Cross-Section of Fluorescent Dye Molecule. *J. Fluoresc.* **2017**, *27*, 1399–1403.
- (23) Nag, A.; De, A. K.; Goswami, D. Two-Photon Cross-Section Measurements Using an Optical Chopper: Z-Scan and Two-Photon Fluorescence Schemes. *J. Phys. B: At., Mol. Opt. Phys.* **2009**, *42*, No. 065103.
- (24) Du, X.; Li, J.; Niu, G.; Yuan, J. H.; Xue, K. H.; Xia, M.; Pan, W.; Yang, X.; Zhu, B.; Tang, J. Lead Halide Perovskite for Efficient Optoacoustic Conversion and Application toward High-Resolution Ultrasound Imaging. *Nat. Commun.* **2021**, *12*, No. 3348.
- (25) Odytek, L. A. K. R. Absorption Coefficients of Bulk GaAs and Si. **2021**; Vol. 29 21, pp 34522–34530.
- (26) Dinu, M.; Quochi, F.; Garcia, H. Third-Order Nonlinearities in Silicon at Telecom Wavelengths. *Appl. Phys. Lett.* **2003**, *82*, 2954–2956.
- (27) Liu, W.; Xing, J.; Zhao, J.; Wen, X.; Wang, K.; Lu, P.; Xiong, Q. Giant Two-Photon Absorption and Its Saturation in 2D Organic-Inorganic Perovskite. *Adv. Opt. Mater.* **2017**, *5*, No. 1601045.
- (28) Schroeder, R.; Ullrich, B. Absorption and Subsequent Emission Saturation of Two-Photon Excited Materials: Theory and Experiment. *Opt. Lett.* **2002**, *27*, 1285–1287.
- (29) Mushtaq, A.; Pradhan, B.; Kushavah, D.; Zhang, Y.; Wolf, M.; Schrenker, N.; Fron, E.; Bals, S.; Hofkens, J.; Debroye, E.; Pal, S. K. Third-Order Nonlinear Optical Properties and Saturation of Two-Photon Absorption in Lead-Free Double Perovskite Nanocrystals under Femtosecond Excitation. *ACS Photonics* **2021**, *8*, 3365–3374.
- (30) Hughes, I. G.; Hase, T. P. A. *Measurements and Their Uncertainties*, 1st ed.; Oxford University Press, 2010.
- (31) Wei, Z.; Guo, D.; Thieme, J.; Katan, C.; Caselli, V. M.; Even, J.; Savenije, T. J. The Importance of Relativistic Effects on Two-Photon Absorption Spectra in Metal Halide Perovskites. *Nat. Commun.* **2019**, *10*, No. 5342.
- (32) Van Stryland, E. W.; Woodall, M.; Vanherzeele, H.; Soileau, M. J. Energy Band-Gap Dependence of Two-Photon Absorption. *Opt. Lett.* **1985**, *10*, 490–492.
- (33) Wherrett, B. S. Scaling Rules for Multiphoton Interband Absorption in Semiconductors. *J. Opt. Soc. Am. B* **1984**, *1*, 67–72.
- (34) Ohara, K.; Yamada, T.; Tahara, H.; Aharen, T.; Hirori, H.; Suzuura, H.; Kanemitsu, Y. Excitonic Enhancement of Optical Nonlinearities in Perovskite CH₃NH₃PbCl₃ Single Crystals. *Phys. Rev. Mater.* **2019**, *3*, No. 111601.
- (35) Garcia, H.; Kalyanaraman, R. Phonon-Assisted Two-Photon Absorption in the Presence of a Dc-Field: The Nonlinear Franz-Keldysh Effect in Indirect Gap Semiconductors. *J. Phys. B: At., Mol. Opt. Phys.* **2006**, *39*, 2737–2746.
- (36) Bahae, M. S.; Hutchings, D. C.; Hagan, D. J.; Van Stryland, E. W. Dispersion of Bound Electronic Nonlinear Refraction in Solids. *IEEE J. Quantum Electron.* **1991**, *27*, 1296–1309.
- (37) Yamada, T.; Aharen, T.; Kanemitsu, Y. Near-Band-Edge Optical Responses of CH₃NH₃PbCl₃ Single Crystals: Photon Recycling of Excitonic Luminescence. *Phys. Rev. Lett.* **2018**, *120*, No. 057404.